X-ray Photoelectron Spectroscopy and Magnetic Studies on the Effect of Pore Size, Wall Thickness, and Wall Composition on Superparamagnetic Cobaltocene Mesoporous Nb, Ta, and Ti Composites

S. Murray,[†] M. Trudeau,[‡] and D. M. Antonelli*,[†]

Department of Chemistry and Biochemistry, University of Windsor, Windsor, Ontario, N9B 3P4, Canada, and Emerging Technologies, Hydro-Québec Research Institute, 1800 Boulevard Lionel-Boulet, Varennes, Quebec, J3X 1S1, Canada

Received June 22, 2000

Recent results in our group demonstrated that mixed oxidation state mesoporous niobium oxide cobaltocene composites display superparamagnetism at certain composition ratios. This was the first report of superparamagnetism in nanoscale molecular ensembles. A series of mesoporous niobium oxide materials were synthesized in order to understand the role of pore size and thickness of the walls in the mesostructure on the magnetic properties. Mesoporous Ti oxide and Ta oxide composites were also synthesized in order to investigate the effect of changing the wall composition on the magnetic properties of this new series of materials. All samples were characterized by X-ray diffraction, nitrogen adsorption, ultraviolet spectroscopy, X-ray photoelectron spectroscoy, scanning electron microscopy, and superconducting quantum interference device magnetometry. The results of this study showed that variation of wall thickness or pore size in the Nb system had little effect on the properties and that superparamagnetism most likely arises from mixed oxidation state cobaltocene grains residing in the individual pores and not from the free electrons in the mesostructure or much larger domains. The Langevin function was applied to the isothermal magnetic data from the Nb composites and gave mean superparamagnetic particle sizes of ca. 14 nm in each system. The Co(II) to Co(III) ratios in these materials were approximately 1:1. The Ti and Ta materials showed no sign of superparamagnetism and only very low levels of neutral cobaltocene in the pores. This suggests that a critical amount of cobaltocene is required to bring about superparamagnetic behavior.

Introduction

Since the discovery of mesoporous MCM-41 in 1992,[1−6] a great deal of research has focused on the synthesis of mesoporous transition metal oxide analogues of these large-pore silica-based materials. Although MCM-41 has high surface area and flexible pore sizes from 20 to 100 Å, useful in applications where fast diffusion of large molecular substrates is essential, it does not possess the variable oxidation states of materials fabricated from transition metal oxides. This property is crucial for many catalytic processes, especially those requiring flexible electrochemical behavior and surface acid sites. Although mesoporous silicates have already shown promise as catalytic supports,[7,8] adsorbents,[9,10] and hosts for intercalation of molecular guest species,[11,12] little work has been carried out on potential applications of related transition metal oxide analogues of these materials.[13−15,16] In 1996 mesoporous Nb,[17−20] Ta,[21] and Ti[22] oxides, materials that fully retain their mesostructure to 400, 600, and 300 °C, respectively, after template removal, were reported and mesoporous Zr oxides,[23−30] Hf oxide,[31] and Mn oxide[32] have also been synthesized. Applications of these

[†] University of Windsor.
[‡] Hydro-Québec Research Institute.

(1) Kresge, C. T.; Leonowicz, M. E.; Roth, W. J.; Vartulli, J. C.; Beck, J. S. *Nature* **1992**, *359*, 710. (b) Beck, J. S.; Vartuli, J. C.; Roth, W. J.; Leonowicz, M. E.; Kresge, C. T.; Schmitt, K. D.; Chu, C. T.-W.; Olson, D. H.; Shepard, E. W.; McCullen, S. B.; Higgins, J. B.; Schlenker, J. L. *J. Am. Chem. Soc.* **1992**, *114*, 10834.
(2) Firouzi, A.; Kumar, D.; Bull, L. M.; Besier, T.; Sieger, P.; Huo, Q.; Walker, S. A.; Zasadzinski, J. A.; Glinka, C.; Nicol, J.; Margolese, D.; Stucky, G. D.; Chmelka, B. F. *Science* **1995**, *267*, 1138.
(3) Chen, C.-Y.; Burkette, S. L.; Li, H.-X.; Davis, M. E. *Microporous Mater.* **1993**, *2*, 27.
(4) Tanev, P. T.; Chibwe, M.; Pinnavaia, T. J. *Nature* **1994**, *368*, 321.
(5) Behrens, P. *Angew. Chem.* **1996,** *108*, 565; *Angew. Chem., Int. Ed. Engl.* **1996**, *35*, 515.
(6) Antonelli, D. M.; Ying, J. Y. *Angew. Chem.* **1995,** *107*, 2202; *Angew. Chem., Int. Ed. Engl.* **1995**, *34*, 2014.
(7) Morey, M.; Davidson, A.; Eckert, H.; Stucky, G. *Chem. Mater.* **1996**, *8*, 486.
(8) Maschmeyer, T.; Rey, F.; Sankar, G.; Thomas, J. M. *Nature* **1995**, *378*, 159.
(9) Baker, J. M.; Dore, J. C.; Behrens, P. J. *Phys. Chem. B* **1997**, *101*, 6226.
(10) Morshige, K.; Nobuoka, K. *J. Chem. Phys.* **1997**, *107*, 6965.
(11) Moller, K.; Bein, T. *Chem. Mater.* **1998**, *10*, 2950.
(12) Wu, C.-G.; Bein, T. *Chem. Mater.* **1994**, *6*, 1109.
(13) Ciesla, U.; Demuth, D.; Leon, R.; Petroff, P.; Stucky, G.; Unger, K.; Schuth, F. *J. Chem. Soc., Chem. Commun.* **1994**, 1387.
(14) Huo, Q.; Margolese, D. I.; Ciesla, U.; Demuth, D. G.; Feng, P.; Gier, T. E.; Sieger, P.; Firouzi, A.; Chmelka, B. F.; Schuth, F.; Stucky, G. D. *Chem. Mater.* **1994**, *6*, 1176.
(15) Antonelli, D. M.; Trudeau, M. *Angew. Chem.* **1999,** *111*, 1555; *Angew. Chem., Int. Ed. Engl.* **1999**, *38*, 1471.
(16) Ying, J. Y.; Mehnert, C. P.; Wong, M. S. *Angew. Chem* **1999**, *111*, 58−82; *Angew. Chem., Int. Ed. Engl.* **1999**, *37*, 664.
(17) Antonelli, D. M.; Ying, J. Y. *Angew. Chem.* **1996,** *108*, 461; *Angew. Chem., Int. Ed. Engl.* **1996**, *35*, 426.
(18) Antonelli, D. M.; Nakahira, A.; Ying, J. Y. *Inorg. Chem.* **1996**, *35*, 3126.
(19) Antonelli, D. M. *Microporous Mesoporous Mater.* **1999**, *30*, 209.
(20) Antonelli, D. M.; Ying, J. Y. *Curr. Opin. Colloid Interface Sci.* **1996**, *1*, 523.
(21) Antonelli, D. M.; Ying, J. Y. *Chem. Mater.* **1996**, *8*, 874.
(22) Antonelli, D. M. *Microporous Mesoporous Mater.* **1999**, *30*, 315.
(23) Reddy, J. S.; Sayari, A. *Catal. Lett.* **1996**, *38*, 219.

10.1021/ic000678f CCC: $19.00
Published on Web 11/23/2000

materials and synthetic routes into new mesoporous materials fabricated from different oxides are no doubt forthcoming.

Recent advances in our group have demonstrated that mesoporous Nb, Ti, and Ta oxides can act as potent electron acceptors while fully retaining their mesostructure.[33,34] This property is of importance to the fabrication of fast ion conduction channels for electrochemical cells and support materials for catalytic reduction of organic species. This electron acceptor property can also be exploited so that mesoporous Nb oxide can act as a charge-balancing sheath stabilizing mixed-oxidation state one-dimensional molecular nanowires of alkali fullerides[35] and organometallic species such as cobaltocene[36] and bisbenzene chromium.[37] Interestingly, neither bisbenzene chromium nor cobaltocene react with Nb_2O_5, and thus, the amorphous nature of the walls is allowing for the presence of acceptor states of energy lower than those in the bulk oxide.[38] This effect is common in amorphous solids, which generally have much wider bandwidths than their crystalline counterparts. Although the bisarene composites are conducting, certain phase compositions of the cobaltocene composites are superparamagnetic, a property normally observed only in soft magnetic materials and ferrofluids. This was the first report of superparamagnetism in a molecular ensemble and demonstrates that the capacity for mesoporous niobium oxide to act as a host for nonstoichiometric molecular clusters can be exploited to lead to materials with highly unusual physical properties. The magnetic behavior of these cobaltocene composites was found to be strongly dependent on the cobaltocene loading level. To further understand what factors govern superparamagnetic transitions in this system, we present a full study of the effect of pore size, wall thickness, and composition of the mesostructure on superparamagnetic behavior. Because of the unpaired electrons in both the walls of the mesostructure and the cobaltocene guest phase, as well as the pore size and compositional flexibility, this is an ideal system to explore magnetic behavior in materials that possess mesoscale periodicity.

Experimental Section

Materials and Equipment. All chemicals unless otherwise stated were obtained from Aldrich. Samples of mesoporous niobium oxide (Nb-TMS1) were obtained from Alfa-Aesar and used without further purification. Mesoporous titanium and tantalum oxides (Ti-TMS1 and Ta-TMS1) were also obtained from Alfa-Aesar and used without further purification. Trimethylsilyl chloride was obtained from Aldrich and distilled over calcium hydride. Nb-TMS1 samples were dried at 100 °C overnight under vacuum and then stirred with excess trimethylsilyl chloride in dry ether for 4−6 h under nitrogen. Cobaltocene was obtained from Aldrich and used without further purification. Nitrogen adsorption data were collected on a Micromeritics ASAP 2010. X-ray diffraction (XRD) patterns (Cu Kα) were recorded in a sealed glass capillary on a Siemens D-500 $\theta-2\theta$ diffractometer. All X-ray photoelectron spectroscopy (XPS) peaks were reference to the carbon C−(C,H) peak at 284.8 eV, and the data were obtained using a Physical Electronics PHI-5500 using charge neutralization. The conductivity measurements were recorded on a Jandel four-point universal probe head combined with a Jandel resistivity unit. The band gaps were calculated from powder UV−visible spectra collected on an Ocean Optics S2000 fiber optics spectrometer equipped with an Analytical Instrument Systems light source emitter with a tungsten halogen lamp and an Ocean Optics UV 0.4 mm, 2M reflection probe. Electron paramagnetic resonance (EPR) samples were prepared under vacuum and the data collected on a Brüker X-band ESP 300E EPR spectrometer. Scanning electron microscope (SEM) analysis was conducted on a JEOL JSM-5800LV scanning microscope. Magnetic measurements were conducted on a Quantum Design superconducting quantum interference device (SQUID) magnetometer MPMS system with a 5 T magnet. All elemental analysis data (conducted under an inert atmosphere) were obtained from Galbraith Laboratories, 2323 Sycamore Drive, Knoxville, TN 37921-1700.

Synthesis. To a suspension of the M-TMS1 (M = Nb, Ti, Ta) in toluene was added 0.5 equiv of cobaltocene calculated on the basis of metal percent as determined from the elemental analysis data. The solution gradually lightened, indicating absorption of the organometallic, and the mesoporous solid went from a light-fawn color to a deep green-black (Nb-TMS1), luminescent green (Ta-TMS1), or dark blue (Ti-TMS1). After several days and additional stirring to ensure complete absorption of the cobaltocene, the reduced material was collected by suction filtration and washed several times with toluene. Once synthesized, all materials were dried in vacuo at 10^{-3} Torr on a Schlenk line until the vacuum gauge showed that all condensable volatiles had been removed. Elemental analysis of the cobaltocene composites synthesized are given below.

Nb-TMS1 with a pore size of 20 Å, $d = 35$ Å treated with excess $CoCp_2$: 22.29% C, 2.64% H, <0.5% N, 0.12% Si, 34.25% Nb, 10.7% Co, 25.95% O. Nb-TMS1 with a pore size of 20 Å, $d = 45$ Å treated with excess $CoCp_2$: 28.24% C, 2.86% H, 0.5% N, 0.18% Si, 31.58% Nb, 23.62% O, 9.75% Co. NbTMS1 with a pore size of 29 Å, $d = 45$ Å treated with excess $CoCp_2$: 13.47% C, 1.9% H, 0.5% N, 0.42% Si, 46.53% Nb, 32.49% O, 4.45% Co. Ta-TMS1 with a pore size of 20 Å, $d = 32$ Å treated with excess cobaltocene: 9.61% C, 1.51% H, 0.62% Si, 59.63% Ta, 26.91% O, 1.72% Co. Ti-TMS1 with a pore size of 24 Å $d = 37$ Å treated with excess cobaltocene: 14.93% C, 2.18% H, 0.17% Si, 36.14% Ti, 42.67% O, 3.91% Co.

Results and Discussion

Previously we showed that samples of Nb-TMS1 can absorb up to 0.5 equiv, calculated on the basis of the percentage of Nb in the sample, of cobaltocene from a toluene solution.[36] These new materials are green to olive-green and retained their structure as determined by XRD and nitrogen adsorption studies. Figure 1b shows the XRD pattern of a sample of Nb-TMS1 (HK pore size of 20 Å, a BET surface area of 947 $m^2\ g^{-1}$, and an XRD peak at $d = 35$ Å, giving a wall thickness of ca. 20 Å) after treatment with 0.5 equiv of cobaltocene. The main peak at $d = 37$ Å is virtually identical to that of the starting material shown in Figure 1a. The nitrogen adsorption isotherm of this new material is shown in Figure 3b, while Figure 3a shows the nitrogen adsorption isotherm of the starting material. The reduction in surface area from 947 to 220 $m^2\ g^{-1}$ is consistent with partial occlusion of the pores by the organometallic. This is also reflected in the reduction of HK pore volume from 0.62 to 0.15 $cm^3\ g^{-1}$. The pore size remained relatively constant at ca. 20 Å. The elemental analysis of this material gave a Co/Nb ratio of ca. 0.5:1, with a carbon value fully consistent with cyclopentadienyl groups by the Co species.

(24) Ciesla, U.; Schacht, S.; Stucky, G. D.; Unger, K.; Schuth, F. *Angew. Chem.* **1996,** *108*, 597; *Angew. Chem., Int. Ed. Engl.* **1996**, *35*, 541.
(25) Ciesla, U.; Fröba, M.; Stucky, G.; Schüth, F. *Chem. Mater*. **1999**, *11*, 227.
(26) Antonelli, D. M. *Adv. Mater*. **1999**, *11*, 487.
(27) Wong, M. S.; Antonelli, D. M.; Ying, J. Y. *Nanostruct. Mater*. **1997**, *9*, 165.
(28) Wong, M. S.; Ying, J. Y. *Chem. Mater*. **1998**, *10*, 2067.
(29) Mamak, M.; Coombs, N.; Ozin, G. *Adv. Mater*. **2000**, *12*, 198.
(30) Hudson, M. J.; Knowles, J. A. *Chem. Mater*. **1996**, *6*, 89.
(31) Liu, P.; Liu, J.; Sayari, A. *J. Chem. Soc., Chem. Commun.* **1997**, 577.
(32) Tian, Z. R.; Wang, J. Y.; Duan, N. G.; Krishnan, V. V.; Suib, S. L. *Science* **1997**, *276*, 926.
(33) Vettraino, M.; Trudeau, M.; Antonelli, D. M. Manuscript submitted.
(34) Vettraino, M.; Trudeau, M.; Antonelli, D. M. *Adv. Mater*. **2000**, *12*, 337.
(35) Ye, B.; Trudeau, M.,; Antonelli, D. M. *Adv. Mater*., in press.
(36) Murray, S.; Trudeau, M.; Antonelli, D. M. *Adv. Mater.* **2000**, *12*, 1339.
(37) He, X.; Trudeau, M.; Antonelli, D. M. Manuscript submitted.
(38) Cox, P. A. *The Electronic Structure and Chemistry of Solids*; Oxford University Press: New York, 1987.

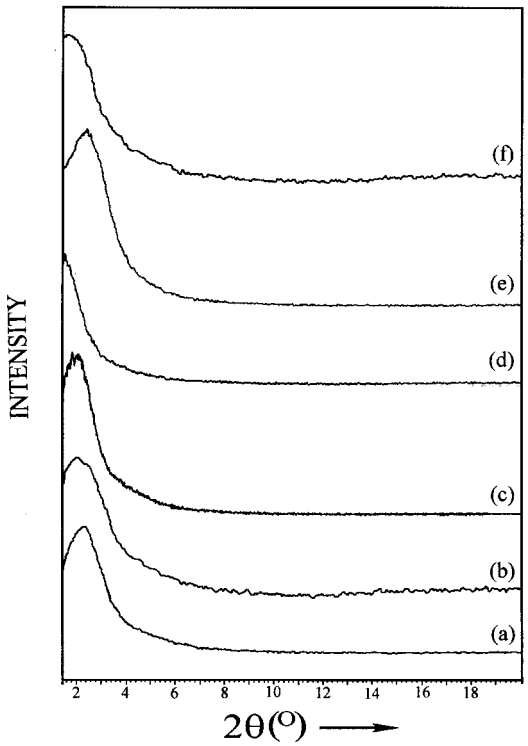

Figure 1. X-ray powder diffraction patterns for trimethylsilated samples of (a) Nb-TMS1 with a pore size of 20 Å and a calculated wall thickness of 20 Å, (b) sample from (a) treated with excess cobaltocene, (c) Nb-TMS1 with a 20 Å pore size and a calculated wall thickness of 32 Å, (d) sample from (c) treated with excess cobaltocene, (e) Nb-TMS1 with a 29 Å pore size and a calculated wall thickness of 20 Å, and (f) sample from (e) after treatment with excess cobaltocene.

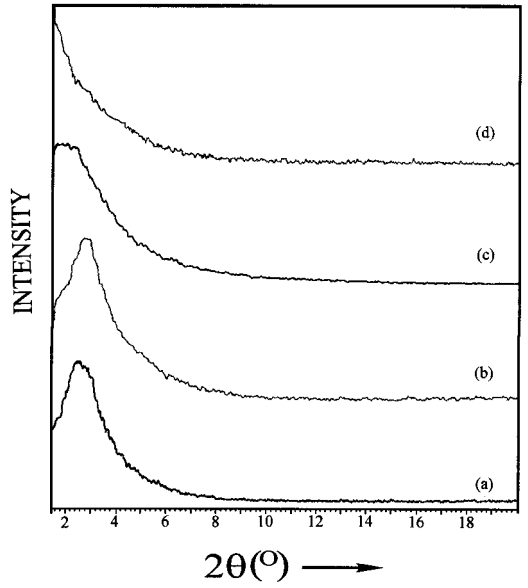

Figure 2. X-ray powder diffraction patterns for trimethylsilated samples of (a) Ta-TMS1, 20 Å pore size, (b) sample from (a) treated with excess cobaltocene, (c) Ti-TMS1, 24 Å pore size, and (d) sample from (c) treated with excess cobaltocene, 23 Å pore size.

To determine the nature of the intercalated cobalt species and the oxidation state of the Nb walls, XPS studies were conducted. The Nb 3d $^5/_2$, $^3/_2$ region of this material shows a peak at 206.8 and 209.6 eV, consistent with partial reduction of the Nb to an average state between +4 and +5 roughly equivalent to that obtained by reduction with 0.1−0.2 equiv of Na−naphthalene.[34]

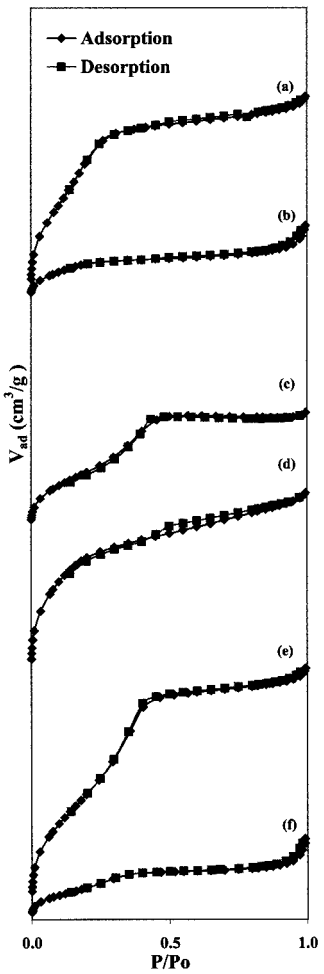

Figure 3. Nitrogen adsorption isotherms of trimethylsilated samples of (a) Nb-TMS1 with a pore size of 20 Å and a calculated wall thickness of 20 Å, (b) sample from (a) treated with excess cobaltocene, (c) Nb-TMS1 with a 20 Å pore size and a calculated wall thickness of 32 Å, (d) sample from (c) treated with excess cobaltocene, (e) Nb-TMS1 with a 29 Å pore size and a calculated wall thickness of 20 Å, and (f) sample from (e) after treatment with excess cobaltocene.

No peaks could be assigned to Nb metal at 202 eV. Figure 5a shows the Co 2p $^3/_2$ region of an XPS spectrum of the sample prepared with a 0.5:1 Co/Nb ratio. The two peaks observed at 779.7 and 781.1 eV correspond exactly to the 2p $^3/_2$ region for cobaltocene and cobaltocinium, respectively.[36] The integrated intensities of these species are 1:1.03, indicating that a small majority of the cobaltocene present is in the Co(III) form. The oxidation of cobaltocene to cobaltocinium is consistent with the reduction of the walls of the mesostructure. No other peaks that could be assigned to cobalt metal or cobalt oxide (778 eV), formed by possible decomposition of the cobaltocene, were observed. The absorption of neutral cobaltocene into the pore structure after the oxidation of the first fraction is a matter of some interest. Although Coulombic forces can readily be invoked to explain why the cobaltocinium resides in the reduced, and therefore negatively charged, pore structure of the material, the fact that this excess neutral cobaltocene cannot be washed out indicates that there are strong host−guest effects at play governed by an equilibrium between solvation by toluene and inclusion in the pore structure. To quantify this relation, we previously defined the host−guest equilibrium constant K_H as the fraction of cobaltocene in the neutral form in the pores relative to that present in the solution.[36] The UV−visible

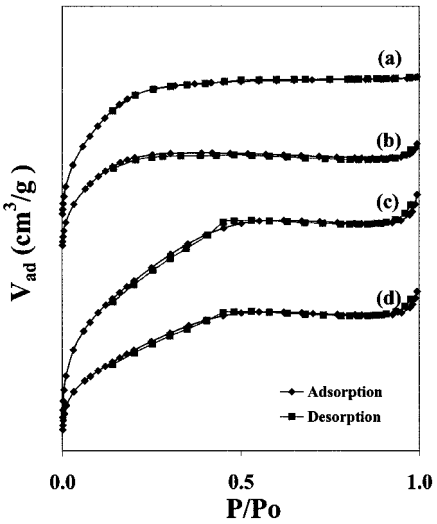

Figure 4. Nitrogen adsorption isotherms of trimethylsilated mesoporous materials (a) Ta-TMS1, 19 Å pore size, (b) sample from (a) treated with excess cobaltocene, (c) Ti-TMS1, 24 Å pore size, and (d) sample from (c) treated with excess cobaltocene.

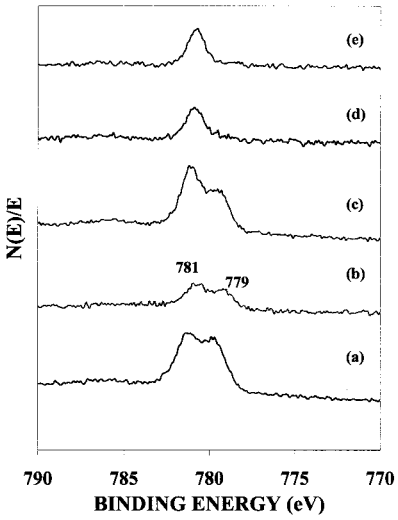

Figure 5. Co 2p $^3/_2$ region of the XPS spectrum of excess cobaltocene composites synthesized from trimethylsilated samples of (a) Nb-TMS1 with a pore size of 20 Å and a calculated wall thickness of 20 Å, (b) Nb-TMS1 with a 20 Å pore size and a calculated wall thickness of 32 Å, (c) Nb-TMS1 with a 29 Å pore size and a calculated wall thickness of 20 Å, (d) Ta-TMS1, 19 Å pore size, and (e) Ti-TMS1, 23 Å pore size.

reflectance spectrum of this material shows peaks at 260, 420, and 580 nm for the Nb−O 2p valence band to conduction band transition (VB−CB) , the cobaltocinium $\pi-\pi^*$ transition, and the transition from the cobaltocene-based impurity band to the conduction band. The assignment of these peaks has been discussed previously.[36] Electron paramagnetic resonance (EPR) spectra of this material show a peak at 3384 G previously assigned to the presence of the free electron in the Nb-based mesostructure and a peak for neutral cobaltocene at 3241 G (Figure 6a).[39] Although bisbenzene chromium and potassium fulleride intercalates of Nb-TMS1 are semiconductors, conductivity measurements of pressed pellets of these cobaltocene samples show that these materials are insulating, as in the case of the alkali metal reduced species.[34] The insulating nature of the niobium oxide mesostructure has been discussed previously and was attributed to Anderson localization of the electrons in the amorphous structure.[36]

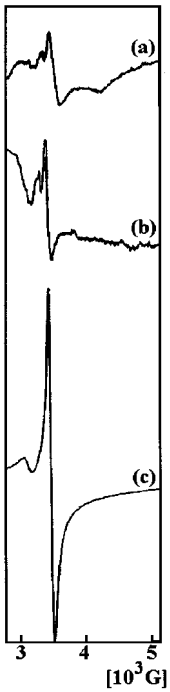

Figure 6. EPR spectra of excess cobaltocene composites synthesized from trimethylsilated samples of (a) Nb-TMS1 with a pore size of 20 Å and a calculated wall thickness of 20 Å, (b) Ta-TMS1, 19 Å pore size, and (c) Ti-TMS1, 23 Å pore size. Hump below 3000 G is due to zero-field effect.

SQUID magnetic studies were conducted and revealed that this material is superparamagnetic, a property normally associated with nanoclusters of soft magnetic materials and ferrofluids. Superparamagnetic particles have single magnetic domains, but they are small enough that thermal fluctuations can easily reverse the direction of their magnetic moment. Figure 7a shows a plot of magnetization versus temperature [*M* versus *T*] from 4 to 100 K. The transition point in the zero-field cooled region of this plot corresponds to a blocking temperature (T_b) of 18 K. Below this temperature the majority of particles are blocked, while above this temperature the material displays standard Curie behavior. The hysteresis in this plot and other *M* vs *T* plots in this study (Figure 7) is not fully understood but may be due to a slight inhomogeneity of magnetic domain sizes. Materials prepared with less than 0.15 equiv of cobaltocene are paramagnetic only and show no magnetic transition. The reason for this is not fully understood; however, it may be related to the concentration of cobaltocene (cobaltocinium has no unpaired electrons and is diamagnetic, while cobaltocene has one unpaired electron and is paramagnetic) in the pores or the particle size of the cobaltocene clusters. This would suggest that the presence of the paramagnetic cobaltocene species in the mesoporous framework, and not that of the diamagnetic cobaltocinium, predominantly contributes to the superparamagnetic phenomenon. This hypothesis is further substantiated by magnetic analysis of materials synthesized with less than 0.15 equiv of cobaltocene. These materials predominantly show the presence of cobaltocinium within the pores with only minor amounts of cobaltocene and do not show superparamagnetic behavior. Figure 8a shows a plot of field versus magnetization [*B* versus *H*] at 300 and 10 K for the same sample. At 300 K there is a rapid increase in isothermal magnetization with increasing applied magnetic field without saturation due to the superparamagnetic relaxation and the noncollinear moment of the surface spins in the superparamagnetic assembly. At 10 K the magne-

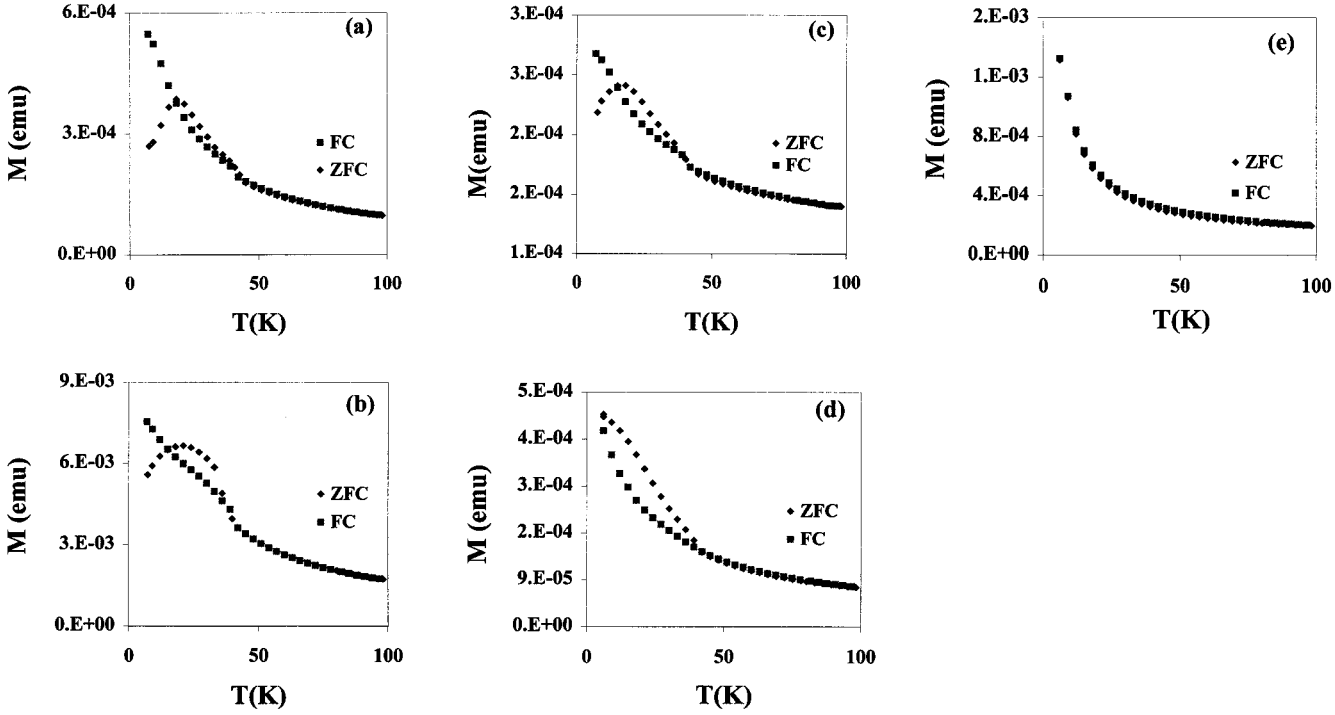

Figure 7. SQUID plots of magnetization versus temperature for excess cobaltocene composites synthesized from trimethylsilated samples of (a) Nb-TMS1 with a pore size of 20 Å and a calculated wall thickness of 20 Å, (b) Nb-TMS1 with a 20 Å pore size and a calculated wall thickness of 32 Å, (c) Nb-TMS1 with a 29 Å pore size and a calculated wall thickness of 20 Å, (d) Ta-TMS1, 19 Å pore size, and (e) Ti-TMS1, 23 Å pore size.

tization increases and the curve exhibits a symmetric hysteresis loop, indicating a transition from superparamagnetic to ferrimagnetic behavior. These data further confirm the superparamagnetic nature of this material. From these data the mean particle size was calculated as 14 nm using the Langevin function[40]

$$M = M_s\left\{\coth(\alpha) - \frac{1}{\alpha}\right\}$$

where

$$\alpha = \frac{\mu_o M_{Co} V H}{k_B T}$$

Since this function assumes spherical particles, this suggests that it is either small spherical regions spanning six or seven pore diameters or 2 nm diameter cigar-shaped cobaltocene phases of volume comparable to that of a 14 nm sphere within a single nanotube that are responsible for the superparamagnetic behavior and not larger domains spanning an entire particle. The relationship between the moles of reductant added to the mesoporous structure and the number of unpaired spins as calculated from the SQUID data is discussed elsewhere.[33] SEM studies were conducted on oxidized samples of these materials shown in Figure 10a, and they show a mean particle size of well over 10 μm in this material with some smaller particles in the 100−500 nm range, assuming the macroscopic structure of the particle was retained on oxidation. Both of these particle size ranges are larger than the calculated superparamagnetic domain size by many orders of magnitude, further supporting the view that the superparamagnetic regions are within one or several adjacent pores and not spanning entire particles, although there is also the possibility that reduction partially damages the structure of the mesopores and that the cobaltocene grains are imbedded in these small defects in the structure. The SEM images of the reduced materials also show unusual macroporous holes in the particles. The presence of these structural facets is not understood but may be related to microbubbles present during the synthesis of the mesoporous starting material. Because of the extreme air sensitivity of these samples, and hence of the cobaltocene domains within the pore structure, we were unable to obtain useful transmission electron microscope (TEM) images of any material in this study.

To probe into the factors contributing to superparamagnetism in this system, a study of variation of pore size, wall thickness, and wall composition was conducted. At this point it was unclear whether the superparamagnetism arises from the cobaltocene clusters within the pore structure or there is some cooperative effect between the magnetic moments of these particles and the unpaired electrons in the walls of the mesostructure. Thus, a material with the same pore size as that above, but with a thicker wall, was prepared in order to gauge the effect of increasing the domain size of the walls while keeping the pore size and hence the maximum cobaltocene cluster size constant. A sample of Nb-TMS1 with an HK pore size of 20 Å, a central peak in the XRD at $d = 45$ Å, and a calculated wall thickness of 32 Å was obtained commercially. The BET surface area of this sample was 450 $m^2\ g^{-1}$. Subsequent prolonged stirring of the material in toluene in the presence of excess cobaltocene led to the isolation of a new gray green material that was collected by suction filtration and dried in vacuo. The XRD and nitrogen adsorption isotherm of this material is shown in Figures 1d and 3d, while Figure 3c shows the nitrogen adsorption isotherm and Figure 1c shows the XRD spectra of the starting material. The XRD showed a peak at 49 Å, and the BET surface area was 230 $m^2\ g^{-1}$. The pore volume dropped from 0.369 to 0.211 cm^3

(39) Ammeter, J. H.; Swalen, J. D. *J. Chem. Phys.* **1972**, *57*, 678.
(40) Padovani, S.; Chado, I.; Scheurer, F.; Bucher, J. P. *Phys. Rev. B* **1999**, *59*, 11887. Wecker, J.; von Helmolt, R.; Schultz, L.; Samwer, K. *IEEE Trans. Magn.* **1993**, *29*, 3087.

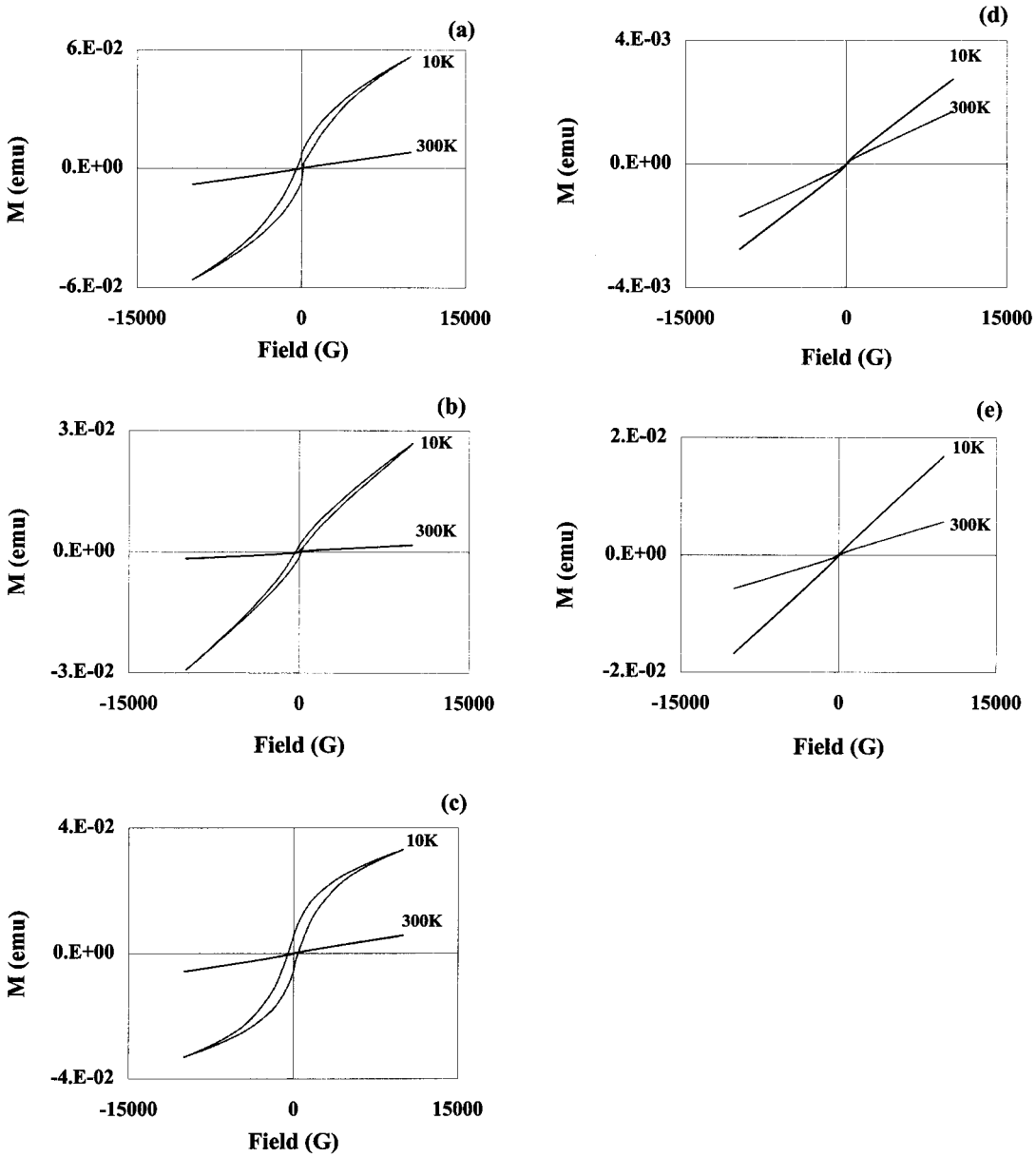

Figure 8. SQUID plots of *B* vs *H* at 10 and 300 K for excess cobaltocene composites synthesized from trimethylsilated samples of (a) Nb-TMS1 with a pore size of 20 Å and a calculated wall thickness of 20 Å, (b) Nb-TMS1 with a 20 Å pore size and a calculated wall thickness of 32 Å, (c) Nb-TMS1 with a 29 Å pore size and a calculated wall thickness of 20 Å, (d) Ta-TMS1, 19 Å pore size, and (e) Ti-TMS1, 23 Å pore size.

g^{-1}, while the ca. 20 Å pore size remained virtually unchanged. These data are consistent with occlusion of the pores due to absorption of cobaltocene. The shift to slightly lower angle of the XRD peak is consistent with a small degree of structural degradation, possibly due to reduction of residual water in the mesostructure to hydroxide. The elemental analysis shows that the Co/Nb ratio has also dropped from 0.5:1 to 0.15:1, as expected from increasing the wall thickness while keeping the pore size the same. The UV reflectance spectrum of this material showed peaks at 260, 460, and 580 nm, consistent with the Nb−O sp VB−CB transition, the cobaltocinium $\pi-\pi^*$ transition, and the Nb 4d$-\pi^*$ impurity band to conduction band transition as noted for the previous cobaltocene intercalate. The EPR spectrum was virtually identical to that of the previous composite, displaying peaks at 3376 and 3239 G for the free Nb electron and neutral cobaltocene, respectively. The Co 2p $^3/_2$ region of the XPS spectrum of this material is shown in Figure 5b and reveals a cobaltocene (779.3 eV) to cobaltocinium (780.9 eV) ratio of 1:1.03 as observed for the first composite. The Nb 3d $^5/_2$, $^3/_2$ region showed a shift to higher binding energy of roughly 0.3 eV compared to the previous sample, consistent with the lesser degree of reduction in these materials expected with the smaller Co/Nb ratio. These data show that an increase in the wall thickness of the material while holding the pore size constant had little or no effect on the ratio of cobaltocene to cobaltocinium in the materials. SQUID magnetic measurements on this material were conducted in order to determine the effect of increasing wall thickness on superparamagnetism. A plot of magnetization versus temperature is shown in Figure 7b. The blocking temperature in this new material has remained at 18 K, indicating that in this sample most of the superparamagnetic particles are blocked until the transition temperature is reached. This indicates that increasing the wall thickness has little effect on the magnetic behavior of the material and that because of this, the free electrons in the wall have only a small or no effect on the magnetic properties of the materials. This tends to support the presence of cigar-shaped clusters within a single pore rather than spherical regions spanning several pore diameters because

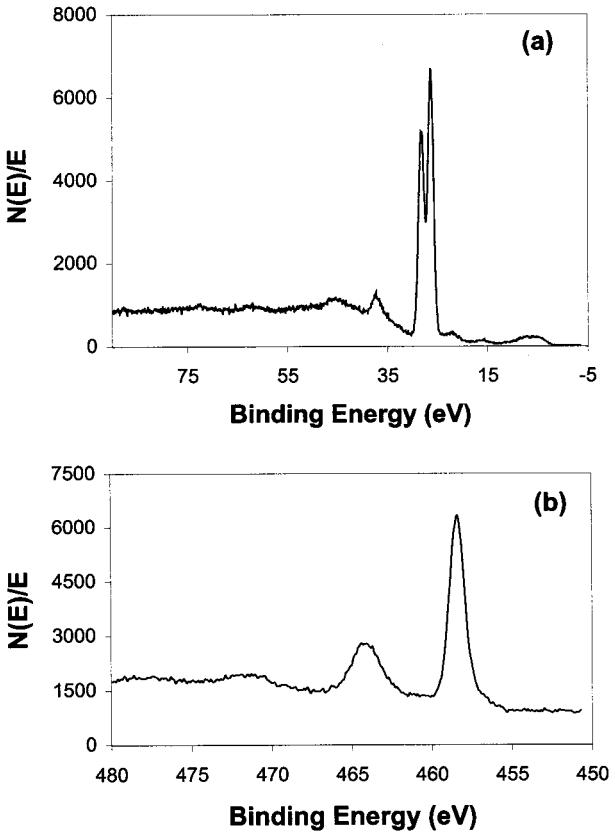

Figure 9. XPS spectra showing (a) Ta 4f $^{7}/_{2}$, $^{5}/_{2}$ region of Ta-TMS1−cobaltocene composite and (b) Ti 2p $^{3}/_{2}$, $^{1}/_{2}$ region of Ti-TMS1−cobaltocene composite.

one would expect some effect of increasing wall thickness in the latter case. The *B* versus *H* curve for this sample is shown in Figure 8b and provides further confirmation of the superparamagnetic properties of this material. Application of the Langevin function gives a mean superparamagnetic particle size of 13.8 nm, indicating that altering the wall thickness did not change the size of the superparamagnetic domains. The SEM results give a mean particle size of ca. 2.5 μm, providing further evidence that the superparamagnetic behavior arises most likely from small clusters within the pores and not larger particles of the material.

To probe the effect of pore size in these materials while keeping the wall thickness constant, a sample of Nb-TMS1 with an HK pore size of 29 Å and a pore volume of 0.655 $cm^3\ g^{-1}$ was obtained. This sample had an XRD peak at 45 Å, a calculated wall thickness of 20 Å, and a BET surface area of 870 $m^2\ g^{-1}$ (Figures 1e and 3e). The subsequent reaction with excess cobaltocene over several days led to a drop in the surface area to 187 $m^2\ g^{-1}$, and the pore size and pore volume were 26 Å and 0.217 $cm^3\ g^{-1}$, consistent with occlusion of the pores with cobaltocene. Figures 1f and 3f show the XRD data and nitrogen adsorption isotherm, respectively. There was a slight loss of definition in the XRD pattern, possibly due to a small degree of structural degradation on reduction of the mesostructured framework. The UV and EPR spectra were virtually identical to those spectra recorded from the other composites in this study. The Co 2p $^{3}/_{2}$ region in the XPS is shown in Figure 5c and reveals that the cobaltocene (779.0 eV) to cobaltocinium (780.9 eV) ratio has changed from 1:1.03 to 1:1.13. The elemental analysis gives a Co/Nb ratio of ca. 0.5:1, and the C content increases from 3.34% to 28.24% on adsorption of the

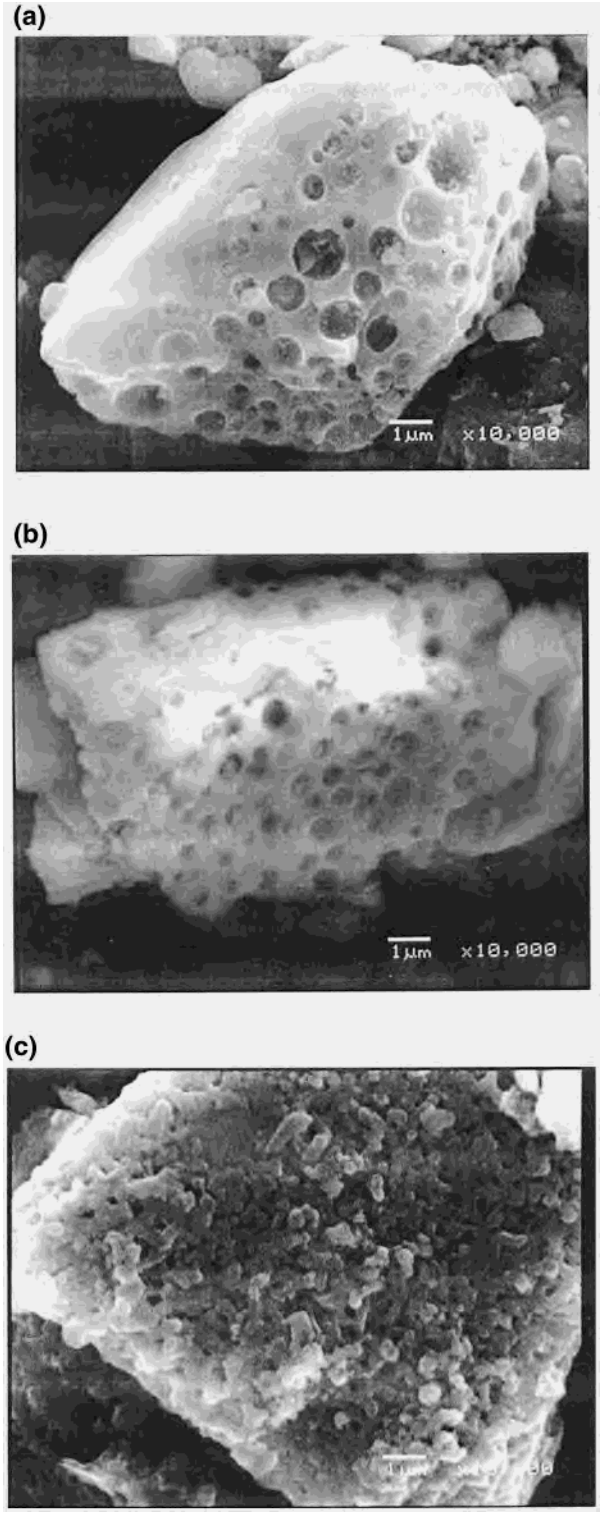

Figure 10. (a) SEM micrograph of cobaltocene composites prepared from (a) Nb-TMS1 with a pore size of 20 Å and a calculated wall thickness of 20 Å, (b) Ta-TMS1, 19 Å pore size, and (c) Ti-TMS1, 23 Å pore size.

organometallic. Thus, the shift to larger pore size has little effect on the adsorption and retention of organometallic in this system. The SQUID *M* versus *T* plot and *B* versus *H* plot are shown in Figures 7c and 8c and show that this material is superparamagnetic with a T_b at 18 K. Application of the Langevin function gives a slightly larger superparamagnetic domain size of 15.3 nm, consistent with an increase in pore size. Again, SEM images

showed that the average particle size of the treated material was over 2 μm, further supporting the argument that the superparamagnetism arises from occluded clusters within one pore and not entire particles.

To investigate the effect of changing the composition of the walls, and hence the oxidizing ability of the structure, samples of Ti-TMS1 and Ta-TMS1 were treated with trimethylsilyl chloride followed by cobaltocene. In a previous study we showed that these materials are also potent electron acceptors, retaining their mesostructure while absorbing up to 1 equiv of reductant.[33] When a sample of trimethylsilated Ta-TMS1 with an HK pore size of 20 Å, a BET surface area of 420 $m^2\ g^{-1}$, a pore volume of 0.116 $cm^3\ g^{-1}$ (Figure 4a), and an XRD peak centered at $d = 32$ Å (Figure 2a) is treated with excess cobaltocene in toluene for several days followed by filtration and extensive washing, a new green material with a virtually identical XRD pattern (Figure 2b), a BET surface area of 311 $m^2\ g^{-1}$, an HK pore size of 19 Å, and a pore volume of 0.055 $cm^3\ g^{-1}$ is formed. The nitrogen adsorption isotherm of this material is shown in Figure 4b. These data are consistent with retention of the mesostructure with concomitant absorption of cobaltocene. The UV reflectance spectrum of this material shows absorbancies at 250 nm for the Ta−O sp VB−CB transition, 480 nm for cobaltocinium, and a broad transition at ca. 590 nm for the Ta 5d−cobaltocene π^* impurity band to CB transition. This confirms the presence of cobaltocinium in the structure and the transfer of an electron to the tantalum oxide mesostructure. Figure 6b shows the EPR of this material with a peak at 3357 G for the free electron. There is also a peak corresponding to cobaltocene; however, this is lower in intensity than in the Nb spectra, perhaps reflecting a decreased amount of this compound in the pore structure. The Co 2p $^3/_2$ region in the XPS is shown in Figure 5d and reveals that although there is cobaltocinium in the material (780.9 eV), there is very little cobaltocene. The elemental analysis shows that the Co/Ta ratio in this material is 0.088:1, indicating that this material has absorbed less organometallic than the Nb materials most likely because of the greater difficulty in reducing tantalum from the +5 to +4 state compared to Nb. This is reflected in the X-ray photoelectron spectrum of the Ta 4f $^7/_2$, $^5/_2$ region (26.6 and 28.5 eV, respectively) shown in Figure 9a, which has shifted only slightly from that of the unreduced compound (26.9 vs 28.7 eV). SQUID magnetic measurements (Figures 7d and 8d) show that this material is paramagnetic with no sign of a superparamagnetic transition at 18 K. We attribute this to the very low loading level of the cobaltocene in this material. SEM studies conducted on oxidized samples of these materials are shown in Figure 10b and show a mean particle size of over 10 μm, similar to that observed in the Nb materials in this study.

When a sample of phosphate-free trimethylsilated Ti-TMS1, with an HK pore size of 24 Å, a BET surface area of 500 $m^2\ g^{-1}$, a pore volume of 0.276 $cm^3\ g^{-1}$ (Figure 4c), and a broad XRD peak centered at $d = 37$ Å (Figure 2c), is treated with excess cobaltocene in toluene for several days followed by filtration and extensive washing, a new dark-blue material with a virtually identical XRD pattern (Figure 2d) and a BET surface area of 298 $m^2\ g^{-1}$ with an HK pore size of 23 Å and a pore volume of 0.182 $cm^3\ g^{-1}$ is formed. The nitrogen adsorption isotherm of this material is shown in Figure 4d. These data are consistent with retention of the mesostructure with concomitant absorption of cobaltocene. The UV reflectance spectrum of this material[41] shows absorbancies at 250 nm for the Ti−O sp VB−CB transition, 480 nm for cobaltocinium, and a broad transition at ca. 590 nm for the Ti 3d−cobaltocene π^* impurity band to CB transition. This confirms the presence of cobaltocinium in the structure and the transfer of an electron to the titanium oxide mesostructure. Figure 6c shows the EPR of this material with a peak at 3387 G for the free electron. There is no visible peak corresponding to cobaltocene, reflecting a decreased amount of this compound in the pore structure. The Co 2p $^3/_2$ region in the XPS is shown in Figure 5e and again reveals that the vast majority of the organometallic is in the cobaltocinium (780.7 eV) and not the cobaltocene form. The elemental analysis shows that the Co/Ti ratio in this material is 0.087:1, indicating that this material has absorbed less cobaltocene most likely because of the greater difficulty in reducing titanium from the +4 to +3 state compared to Nb. This is reflected in the XPS of the Ti 2p $^3/_2$, $^1/_2$ region (458.3 and 464.4 eV, respectively) shown in Figure 9b, which is virtually identical to that in the unreduced compound (459.3 vs 464.9 eV). SQUID magnetic measurements (Figures 7e and 8e) of this material show that it is paramagnetic with no sign of a superparamagnetic transition. We attribute this to the very low loading level of the cobaltocene in this material. SEM studies conducted on oxidized samples of these materials are shown in Figure 10c and show the presence of large particles in the 5−10 μm range as well as smaller particles in the 100−500 nm range.

Conclusion

The results presented herein show that superparamagnetism in mesoporous transition metal oxide−cobaltocene composites is strongly dependent on loading of the cobaltocene as well as on the Co(II)/Co(III) ratio in these materials. The large-pore niobium materials are able to absorb more cobaltocene, while the materials with smaller pores do not absorb as much. The cobaltocene-to-cobaltocinium ratio in these materials increases from 1:1.03 (for larger-pore materials) to 1:1.13 (for small-pore materials), and hence, the degree of cobaltocene absorbed is also dependent on the amount of cobaltocinium present within the sample. Small-pore Ta and Ti materials, which are more difficult to reduce, react with less cobaltocene, have a much greater relative amount of cobaltocinium present in the pore structure (relative to large-pore niobium materials) and because of this show no superparamagnetic transition. This makes absorption of further amounts of cobaltocene less favorable. The thickness of the walls had no effect on the superparamagnetic behavior, indicating that the superparamagnetism depends on the unpaired cobaltocene electrons and not the free electrons in the walls of the structure. Studies are ongoing to find different but related systems that display this behavior, allowing us to further investigate the nature of the superparamagnetic molecular ensembles in these new composites.

Acknowledgment. NSERC and The Ontario Premier's Research Excellence Award program are thanked for funding. Mr. Robinson is thanked for his help with the XRD and SEM data analysis, and Mr. Xun He is thanked for his help with EPR studies.

IC000678F

(41) Stone, V. F., Jr.; Davis, R. *Chem. Mater*. **1998**, *10*, 1468.